International Journal of Heat and Mass Transfer 205 (2023) 123905

Contents lists available at ScienceDirect

International Journal of Heat and Mass Transfer

journal homepage: www.elsevier.com/locate/hmt

A compact jet array impingement cooling system driven by integrated piezoelectric micropump

Yiwen Fan, Xinfeng Zhang, Linyi Xiang, Yanhua Cheng, Xiaobing Luo*

School of Energy and Power Engineering, Huazhong University of Science and Technology, Wuhan 430074, China

ARTICLE INFO

Article history:
Received 28 August 2022
Revised 24 November 2022
Accepted 24 January 2023

Keywords:
Jet impingement cooling
Piezoelectric micropump
Thermal management

ABSTRACT

Thermal management has become a bottleneck for high-power electronics due to high heat flux. Liquid cooling has been developed as an effective way to dissipate the heat of electronic devices. However, the existing liquid cooling systems are mostly too bulky to be applied in the miniaturized devices with very limited installation space. In this work, by integrating jet impingement cooling with piezoelectric micropump, we proposed a compact liquid cooling system that simultaneously enables high heat removal capability and tiny volume. The functions of jet array impingement cooling and coolant pumping are realized in a single component with an external dimension of 40 mm × 40 mm × 10 mm. The thermal performance of the system was investigated by experiments. The results show that the convective heat transfer coefficient achieves 20572 $W{\cdot}m^{-2}{\cdot}K^{-1}$ at a heat flux of 91.5 W/cm^2. And the electric power consumption of the system is only 0.023 W under a heat load of 200 W (50 W/cm^2). Simulations, which agree well with experiments, were further employed to study the transient heat transport process. This novel jet impingement cooling system driven by integrated piezoelectric micropump is compact and efficient, which provides a promising solution for the thermal management of high-power, miniaturized electronic devices.

1. Introduction

With the increasing integration of electronics, the temperature of chips continues to rise due to higher heat flux. High temperature leads to poor performance and high failure rates of chips [1–4], which restrict the development of electronics. To dissipate the tremendous heat from small chips, various efficient liquid cooling technologies have been developed, such as microchannel cooling [5–7], spray cooling [8–10], and jet impingement cooling [11–13]. With the advantages of high thermal performance, efficiency, and flexibility, liquid cooling systems have been widely used in electric cars [14,15] and data centers [16,17]. However, thermal management systems utilizing liquid cooling technologies usually have large volume, which restricts their applications in small spaces, such as aerospace and portable electronics. A compact liquid cooling system is thus of great importance.

Liquid cooling system consists of the following functional components: pump, heat sink, and heat exchanger. Substantial research efforts have focused on the miniaturization of these components [18–20]. Duan et al. developed a high-performance mechanical micropump for liquid cooling systems with an external dimension of ϕ43 mm × 65 mm [21]. Yueh et al. applied a miniature piezoelectric micropump (30 mm × 15 mm × 3.8 mm) to an active fluidic cooling system [22]. Jung et al. developed a silicon microchannel cold plate with low profile for power electronics [23]. To reduce the size and weight of the thermal management system, Kwon et al. developed a 1 cm^3 heat exchanger by electrical-discharge machining [24]. These works successfully decrease the size of the individual components and save some space for the mount of the cooling system. However, it is still not enough for those extremely room-limited applications.

Since the sizes of single components have almost been reduced to the limit, some new schemes of components integration are developed to further decrease the total volume of liquid cooling systems [25–28]. Among these schemes, integrating heat sink with micropump is a feasible solution, where piezoelectric micropump is employed as a substitute of conventional micropump due to its unique advantages in integration [29,30]. For example, Ma et al. developed a mini-channel cold plate integrated with a piezoelectric micropump for laptops and dissipated a heat load of 60 W [31]. Tang et al. experimentally investigated the thermal performance of an integrated heat sink with a piezoelectric pump, which

* Corresponding author.
E-mail address: luoxb@hust.edu.cn (X. Luo).

https://doi.org/10.1016/j.ijheatmasstransfer.2023.123905
0017-9310/

Nomenclature

JAICIPM	jet array impingement cooling with integrated piezoelectric micropump
HTC	heat transfer coefficient, ($W{\cdot}m^{-2}{\cdot}K^{-1}$)
t	time, (s)
t_{cycle}	time of one cycle, (s)
T	temperature, (K)
Q	flow rate, (mL/min)
P	pressure, (kPa)
q	heat flux, (W/cm^2)
h	heat transfer coefficient, ($W{\cdot}m^{-2}{\cdot}K^{-1}$)
R	Thermal resistance, (K/W)
λ	thermal conductivity, ($W{\cdot}m^{-1}{\cdot}K^{-1}$)
ρ	density, (kg/m^3)
μ	viscosity, (mPa·s)
c_p	specific heat capacity, ($J{\cdot}kg^{-1}{\cdot}K^{-1}$)
ΔT	surface temperature rise, (K)
A	the area of the cooling surface
Subscript	
in	inlet
out	outlet
max	maximum
s	surface
j	jet
r	return
ave	average
v	volume
w	water
c	copper

achieved a convective heat transfer coefficient of 4800 $W{\cdot}m^{-2}{\cdot}K^{-1}$ [28]. These previous studies demonstrate the feasibility of pump-integrated liquid cooling system. However, there are still considerable room for the enhancement of the heat dissipation capability of the cooling system. For instance, the heat sink can be designed according to the driving characteristics of piezoelectric micropumps. Piezoelectric micropumps show a relatively high output pressure but a low flow rate due to the driving characteristic of the piezoelectric actuator [29,32]. Therefore, it's greatly significant to develop an integrated cooling system, which can make full use of the high pressure to achieve high thermal performance under a low flow rate.

In this work, we propose an effective way to provide high heat removal ability and reduce the size of the liquid cooling system by integrating jet impingement cooling with piezoelectric micropump. The jet impingement cooling system ejects high-speed coolants onto the cooling surface through small nozzles and produces a high convective heat transfer coefficient with a relatively low flow rate. A compact jet array impingement cooling system with integrated piezoelectric micropump (JAICIPM) was designed, fabricated, and tested. The thermal performance of the JAICIPM was investigated by experiments and simulations.

2. Methods

2.1. Design and fabrication of JAICIPM

Fig. 1(a) shows the schematic diagram of the JAICIPM. The JAICIPM is mainly composed of a piezoelectric actuator and a 3D printed base with internal flow channels and nozzles. The piezoelectric actuator is fixed onto the base by the cover and screws. All the interfaces are sealed by O-rings. Two external check valves, designed as our previous study [33], are connected to the inlet and outlet to control the direction of fluid flow. Fig. 1(b) shows the flow path of the coolant. Jet array impingement cooling with distributed returns is designed to maintain uniform cooling. The coolant flows into the JAICIPM from the inlet and is then distributed to the jet nozzles through the channels. The coolant is directly ejected onto the cooling surface and flows out through the return nozzles. The arrangement of the impinging jets and returns is shown in Fig. 1(c). The area of the jet impinging is 20 mm × 20 mm. The distance between two adjacent nozzles S is 4 mm. Thus, there are 25 impingement nozzles and 16 return nozzles. The diameters of the jet nozzles d_j and return nozzles d_r were designed as 0.4 mm and 1.0 mm, respectively. Previous studies indicate that optimal heat transfer could be obtained when H/d_j is in the range of $2 \sim 4$ for jet array impingement [34]. The height of the jet cavity H is designed as 0.8 mm. The base was fabricated by Stereolithography (SLA) 3D printing. The 3D printing technology enables the complicated array jet impingement structures in a small size without assembly and sealing. Fig. 1(d) and Fig. 1(e) show the pictures of the 3D printed base and the assembled JAICIPM. The dimensions of the JAICIPM were examined by a microscope. The diameter of the nozzles is measured to be $d_j = 425 \pm 28$ μm and $d_r = 1023 \pm 26$ μm, respectively. The external dimension of JAICIPM is 40 mm × 40 mm × 10 mm (16 cm^3) after assembly. The detailed parameters of the components are shown in Table 1.

Table 1
Material and size of the components.

Component	Material	Dimensions (mm)
Cover	Stainless steel	40 × 40 × 2.5
Piezoelectric actuator	Brass plate and PZT ceramic	ϕ35 × 0.53
3D printed base	Photocurable resin	40 × 40 × 7.5

With the vibration of the piezoelectric actuator under AC voltage, the coolant is sucked into and discharged from the chamber of the JAICIPM periodically. Due to the actions of the check valves, the flow of the coolant is unidirectional. As the volume of the chamber increases, the coolant is sucked into the chamber through the inlet and nozzles, and ejected onto the cooling surface to extract the generated heat. As the volume decreases, the coolant is discharged to take the heat away. Then, electronics can be cooled continuously in the repeated process. The piezoelectric actuator is driven by a sine waveform in this study. Therefore, the ideal transient flow rate of the inlet and the outlet is shown as Fig. 2. The flow rate varies from 0 to π times the average flow rate in a half cycle, and remains 0 in another half cycle. The flow rate of the jet impingement is equal to the flow rate of the inlet. The changing flow rate leads to a changing thermal performance in the cycle. Although the jet impinging is intermittent, the cooling performance of the JAICIPM could remain stable because of the thermal capacity and a high driving frequency.

2.2. Numerical simulation

Three-dimensional Finite Volume Method simulations were conducted to evaluate the thermal performance of the JAICIPM. Due to the driving characteristics of the piezoelectric micropump, the velocity of the jet impinging is changing at different periods. Therefore, transient simulations are necessary to investigate the transient thermal performance. Steady simulations were performed before the transient simulations to initialize the cases. RNG k-epsilon turbulence model with enhanced wall treatment was chosen to simulate the flow field according to previous studies [35,36]. Pressure-based solver with SIMPLE method was selected, and the convergence criteria is 1×10^{-6} for the energy term and 1×10^{-3} for the others. The boundary conditions setup is shown in Fig. 3(a). The bottom surface of the chip was set to a constant heat flux of

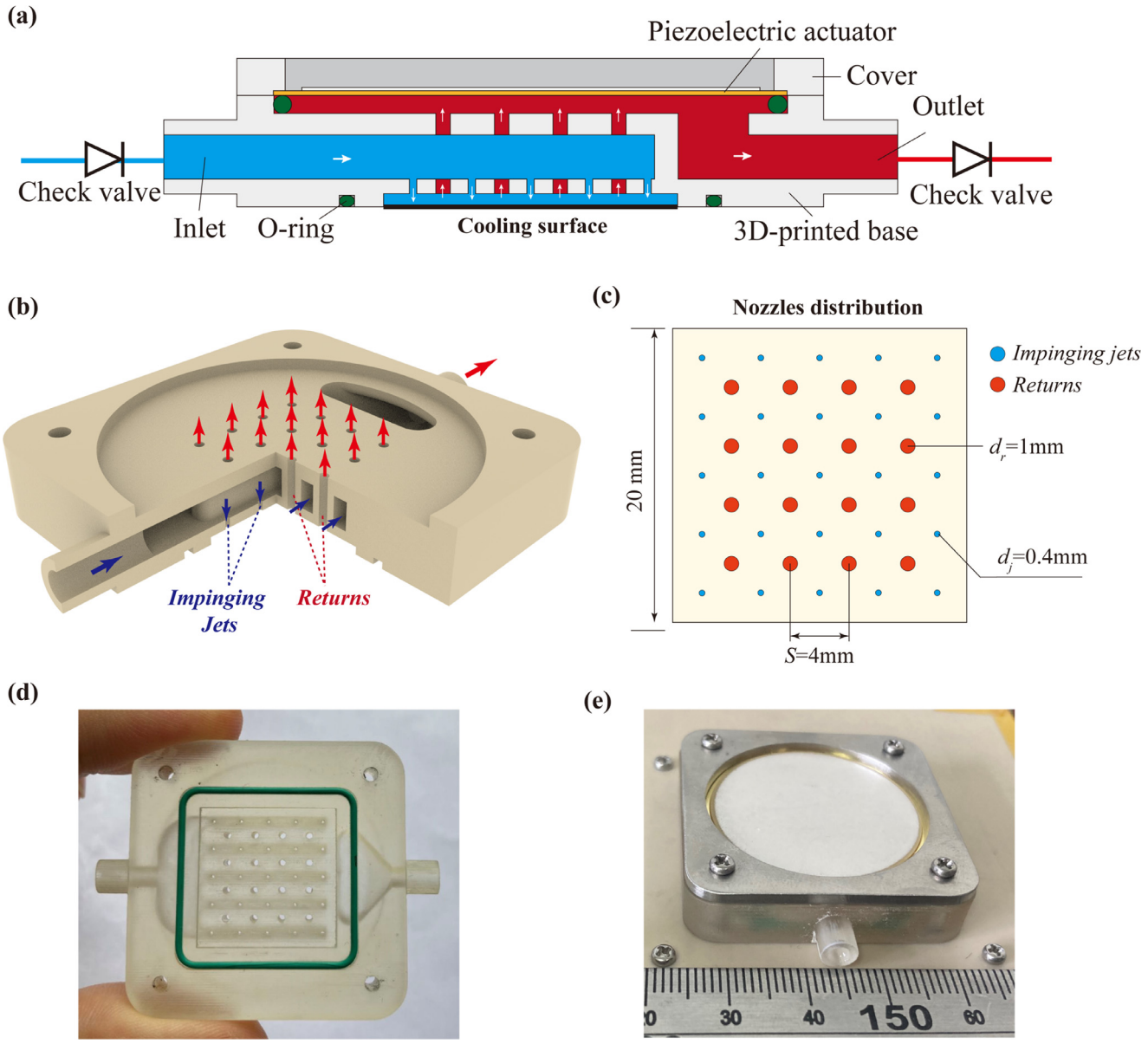

Fig. 1. (a) Schematic diagram of the structure of the JAICIPM, (b) the flow path of the coolant, (c) the arrangement of the impinging jets and returns, (d) the picture of the 3D printed base, (e) the picture of the assembled JAICIPM.

Table 2
The physical property parameters of materials used in the numerical simulation.

Material	λ (W/(m·K))	ρ (kg/m^3)	μ (mPa·s)	c_p (J/(kg·K))	T_{in} (°C)
Water	0.61	992.0	Temperature- varied	4179	25
Copper	380	8960	/	394	/

50 W/cm^2. The inlet boundary was set to velocity inlet with an UDF, and the outlet was set to pressure outlet. The other walls were set adiabatic. The inlet temperature and the reference temperature were set to 298.15 K. The simulated chip was set as copper and the coolant was the deionized water. The physical property parameters of the materials used in the simulation are listed in Table 2. As the viscosity of water varies greatly with the temperature, the viscosity was set to piecewise interpolation. The detailed calculation of viscosity can be found in the supplementary material. Except viscosity, the thermophysical properties of water is relatively stable with the change of temperature. Therefore, the other thermophysical properties was based on the inlet temperature. The time step of the transient simulation was set to 1/20 t_{cycle}, which is 1.11 ms when the driving frequency is 45 Hz. The number of time steps is set to 200 to simulate 10 cycles totally and the maximum iterations for each time step is 150 to insure convergence.

The mesh of the numerical simulation is shown in Fig. 3(b). To meet the $y+$ requirements of the enhanced wall treatment, the grid height of the first layer was set to 0.01 mm, and the growth factor was set to 1.2. The grid independence was done by changing the size of the grids with steady simulations at a flow rate of 250 mL/min and a heat load of 200 W. The pressure drop and the average surface temperature rise of the JAICIPM were simulated with 2193,030, 4928,429 and 6871,256 grids. As shown in Table 3,

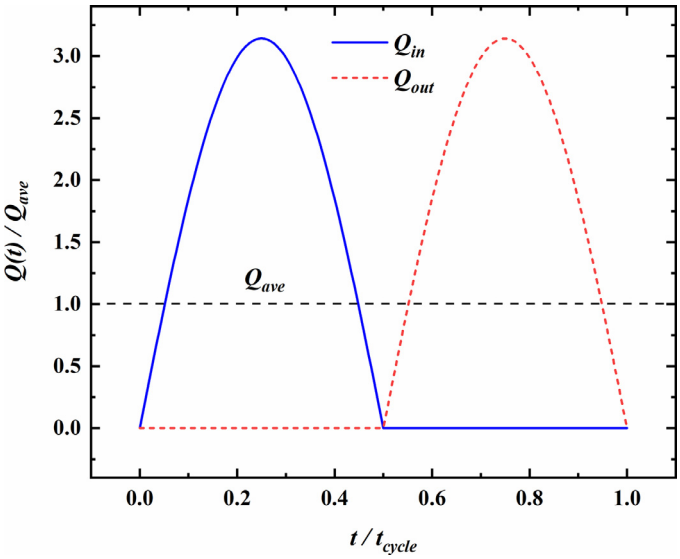

Fig. 2. The ideal transient flow rate of the JAICIPM.

Table 3
Verification of grid independence.

Number of grids	Pressure drop (kPa)	Average wall temperature rise (K)
2193,030	2.59	34.0
4928,429	2.59	34.1
6871,256	2.59	34.1

the discrepancies of pressure drop and average surface temperature rise are no more than 1%. Considering the calculation costs and accuracy, the grids of 4928,429 was chosen in this study.

2.3. Experimental setup

In order to evaluate the thermal performance of the JAICIPM, a test facility was constructed, which is depicted in Fig. 4. To simulate the high-power chip, four heating rods are inserted into the copper block (Pure copper, 380 W/m·K), which can generate a heat load of 100 ~ 400 W. The area of the cooling surface is 4 cm^2 (20 mm × 20 mm), and the heat flux varies from 25 ~ 100 W/cm^2 correspondingly. A framework made by Poly-ether-ether-ketone (PEEK, 0.29 W/m·K) is utilized to support the components and provide heat insulation. The JAICIPM is fixed onto the framework by screws. As for the driving of the JAICIPM, the power signal generator (Aigtek, ATG2031, China) generates a sinusoidal signal to drive the piezoelectric actuator and the power consumption is recorded by a power meter (HIOKI, PW3335, Japan). The voltage of the driving signal is set as 100 ~ 300 Vpp (35 ~ 106 VAC). Then, the coolant can be circulated with the JAICIPM and pipes, bringing the generated heat from the chip to the water tank. The water tank is equipped with a radiator which maintains the water inside at 25 ~ 30 °C. Three K-type thermocouples (T-K-36, ETA, China) are inserted into the copper clock to evaluate the thermal performance of the jet impingement cooling. And two thermocouples are used to measure the temperature of the coolant at the inlet and outlet. All these temperatures are recorded by a data acquisition system (2700, Keithley, US). The detailed dimensions of the heat source are shown in Fig. 5. The distance between the thermocouple 1 and the upper surface is 2 mm. And the thermocouples were arranged with a spacing of 5 mm. Because of the thermal diffusion process, the temperature measurement didn't fluctuate with time in the experiments although the flow and surface temperature varies sinusoidally. Only average thermal performance could be obtained by the experiments.

2.4. Data analysis

According to the one-dimensional Fourier's law of heat conduction, the effective heat flux of the cooling surface can be calculated

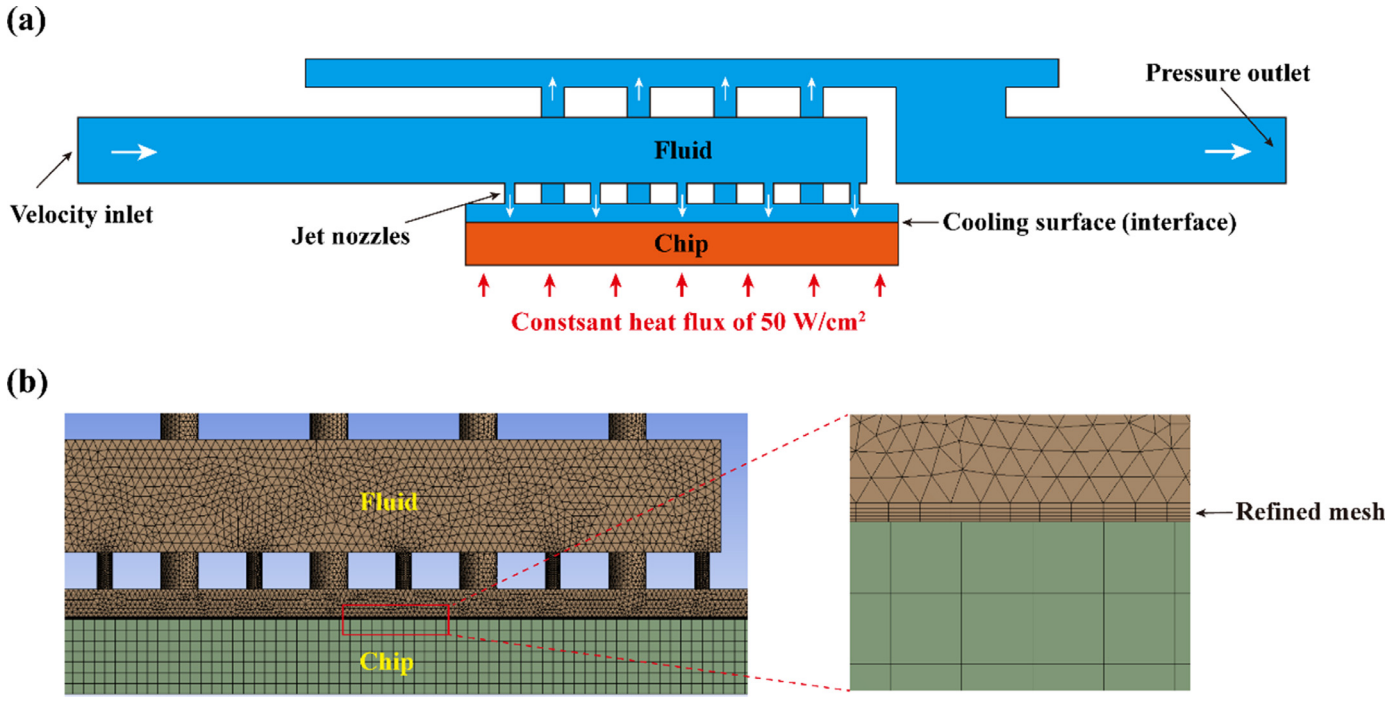

Fig. 3. Setup of the numerical simulation: (a) the boundary conditions, (b) the mesh.

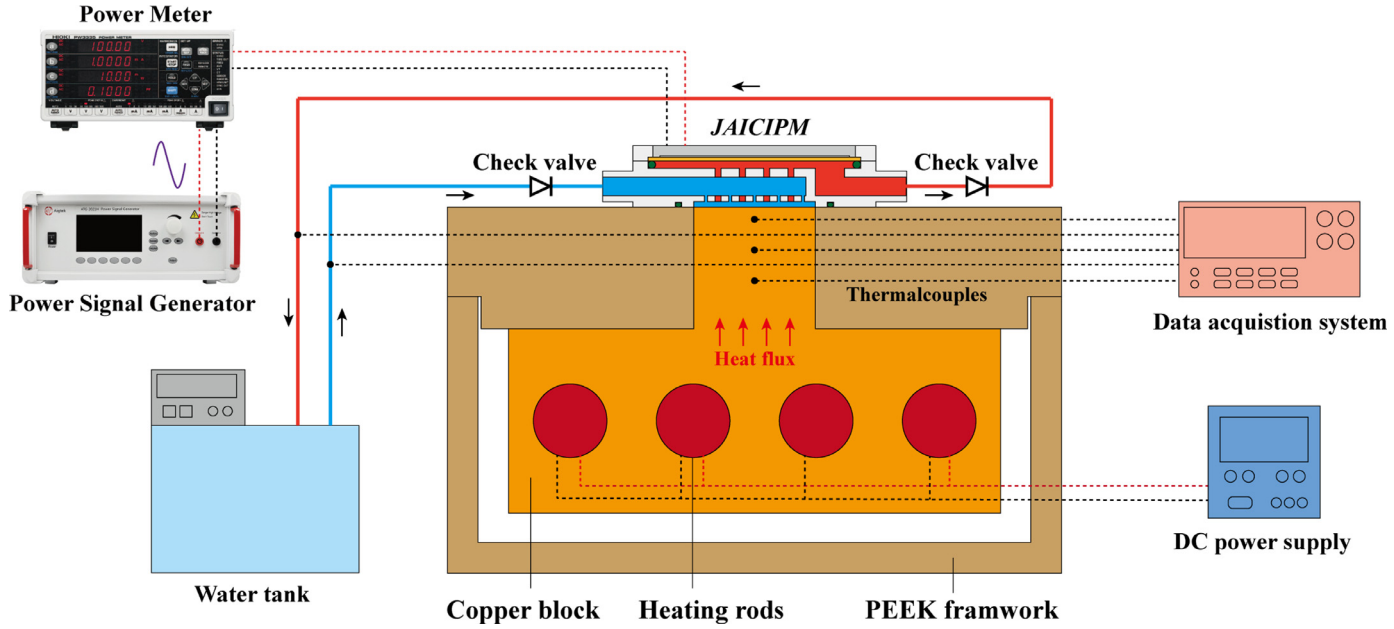

Fig. 4. The schematic of the test facility.

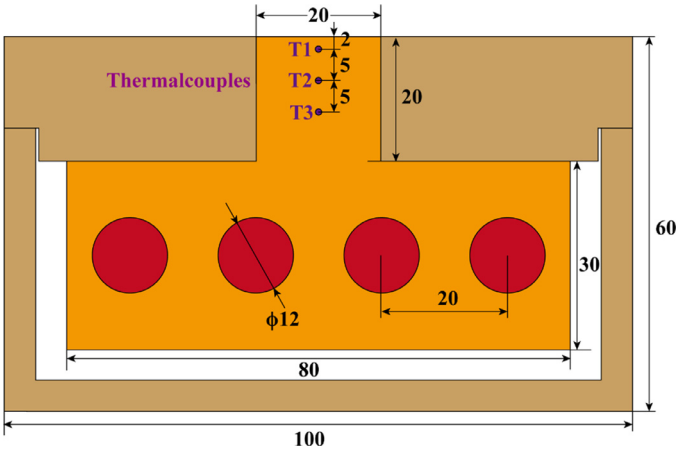

Fig. 5. The dimensions of the heat source.

with the temperature gradient of the copper block:

$$q = -\lambda_c \frac{dT}{dy} \tag{1}$$

where λ_c is the thermal conductivity of the copper block, y is the vertical distance from the cooling surface.

The temperature of the cooling surface T_s, the temperature rise ΔT, and the heat transfer coefficient h can be calculated as:

$$T_s = T_1 + y_1 \frac{dT}{dy} \tag{2}$$

$$\Delta T = T_s - T_{in} \tag{3}$$

$$h = \frac{q}{\Delta T} \tag{4}$$

where T_{in} is the inlet coolant temperature, y_1 is the distance between the surface and the thermocouple 1.

Then, the thermal resistance of the JAICIPM can be calculated as:

$$R = \frac{1}{hA} \tag{5}$$

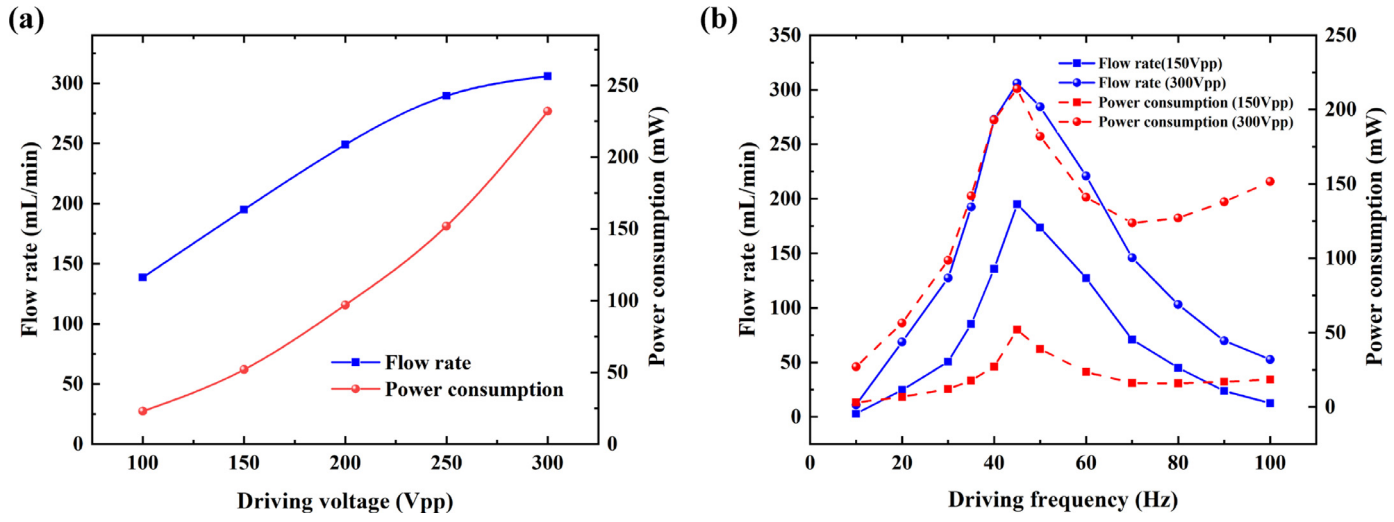

Fig. 6. Flow rate and power consumption of the JAICIPM: (a) at different driving voltages, (b) at different driving frequencies.

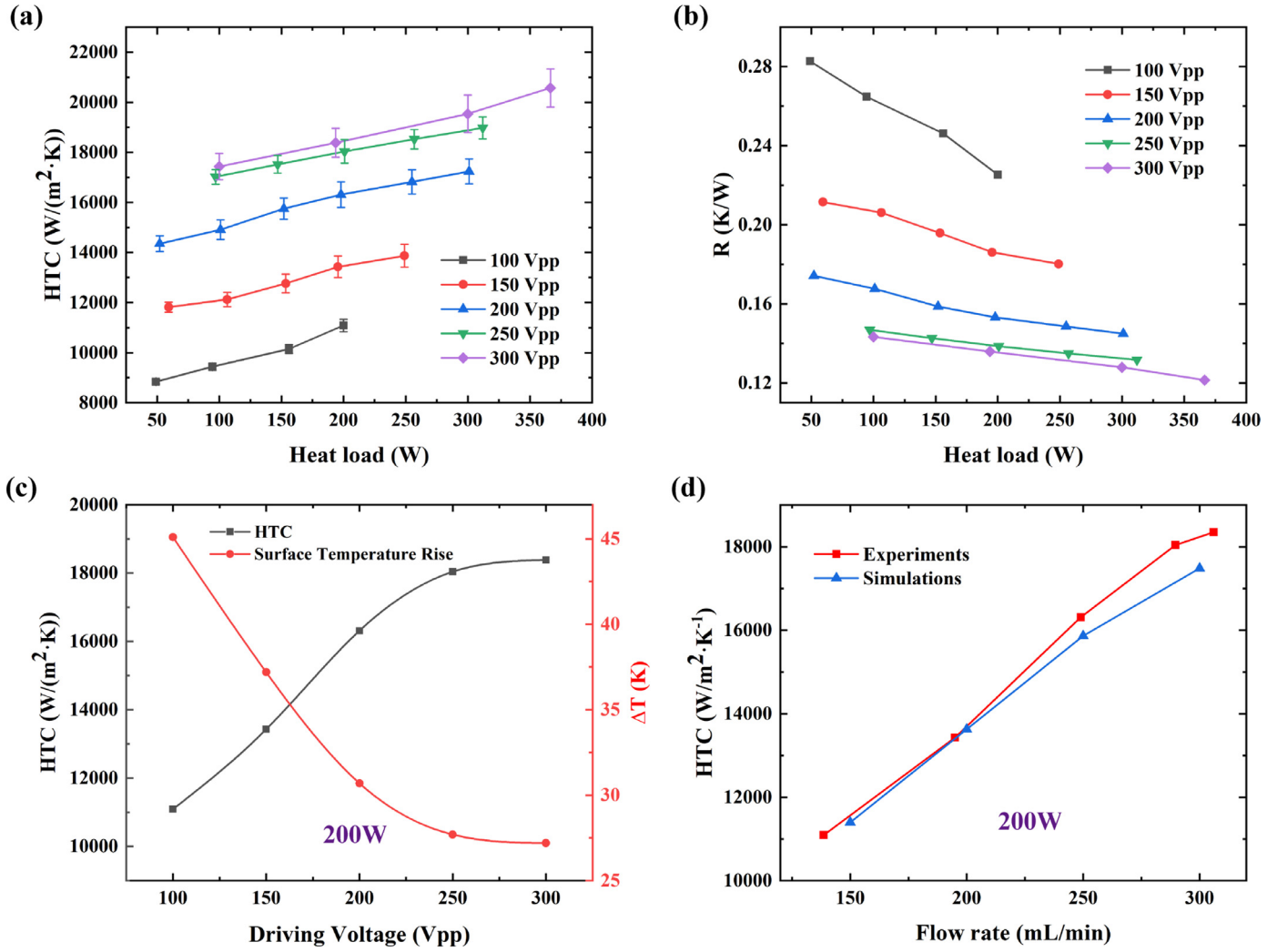

Fig. 7. Thermal performance of the JAICIPM.

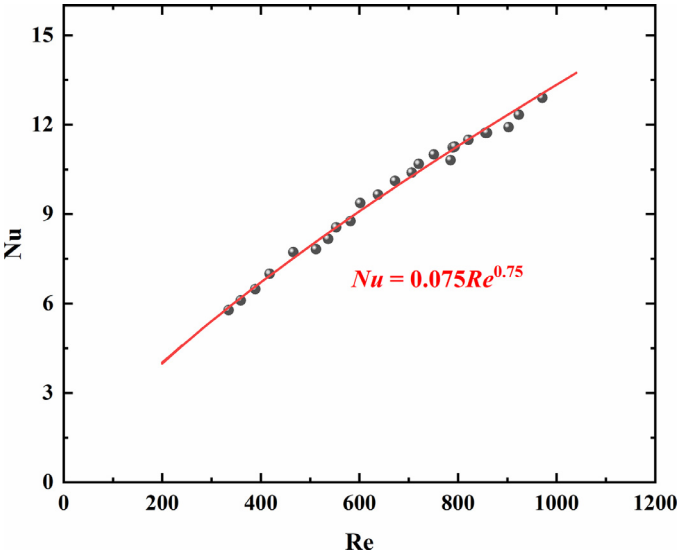

Fig. 8. Nusselt number versus Reynolds number.

As the coolant remains single phase in the experiment, the volumetric flow rate of the JAICIPM can be calculate by the conservation of energy,

$$Q_v = \frac{qA}{\rho c_p (T_{out} - T_{in})} \tag{6}$$

where c_p is the thermal capacity of water, T_{in} is the inlet temperature, T_{out} is the outlet temperature.

As for the calculations of thermal performance with numerical results, T_s is the area average surface temperature, which is calculated as

$$T_s = \frac{\int T_{loc} dA}{A} \tag{7}$$

where T_{loc} is the local temperature of the surface.

The transient heat transfer coefficient is calculated as:

$$h(t) = \frac{q}{(T_s(t) - T_{in})} \tag{8}$$

The impingement velocity is calculated as

$$V_j = \frac{Q_v}{N \times \frac{1}{4}\pi d_j^2} \tag{9}$$

The Reynold and Nusselt number are defined as

$$Re = \frac{\rho_w V_j d_j}{\mu} \tag{10}$$

$$Nu = \frac{h d_j}{\lambda_w} \tag{11}$$

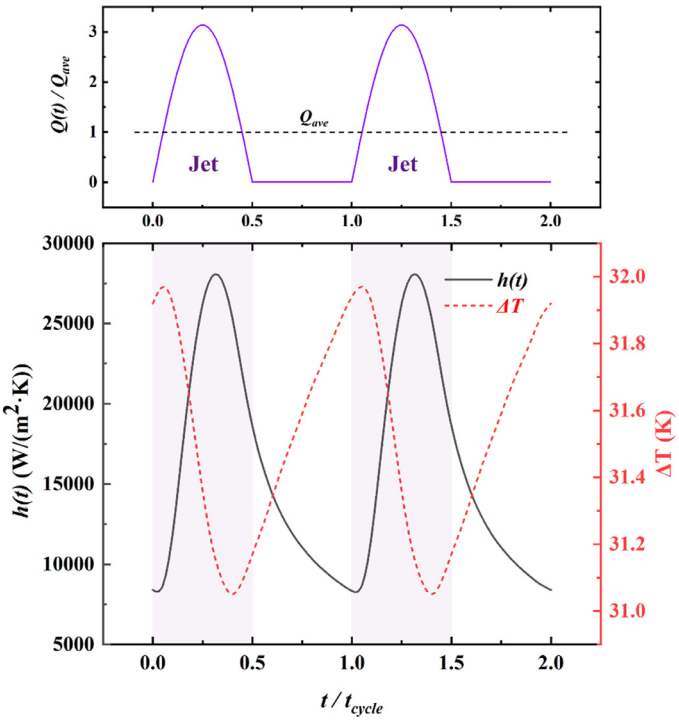

Fig. 9. Transient HTC and surface temperature rise.

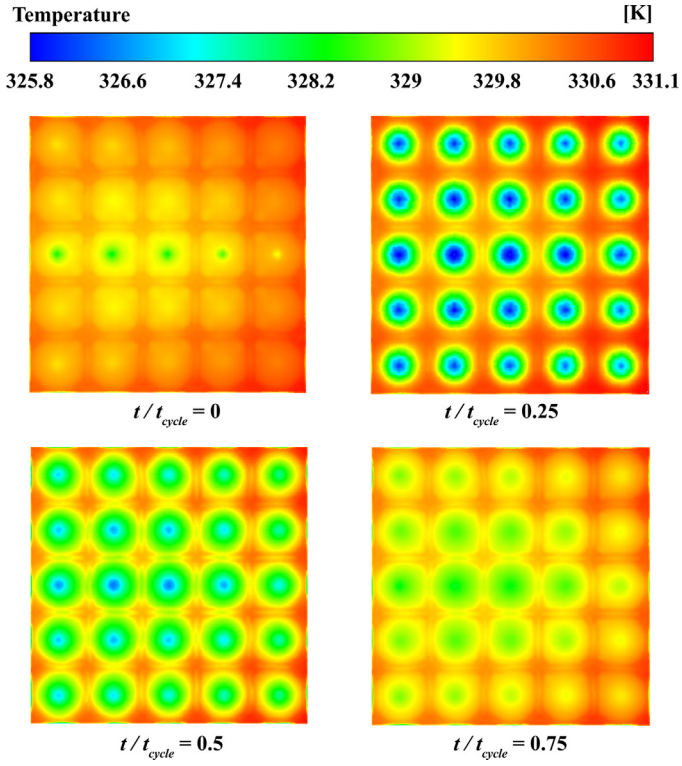

Fig. 10. Temperature distribution of the surface at different times.

2.5. Uncertainty analysis

The absolute error of the K-type thermocouple is ±1.1 °C and the dimensional error of copper block is ±0.1 mm. According to the error-transfer methodology, the uncertainty of heat flux and average heat transfer coefficient can be calculated as:

$$\frac{U_q}{q} = \sqrt{\left(\frac{U_{(T_3-T_1)}}{T_3-T_1}\right)^2 + \left(\frac{U_{(y_3-y_1)}}{y_3-y_1}\right)^2} \tag{12}$$

$$\frac{U_h}{h} = \sqrt{\left(\frac{U_q}{q}\right)^2 + \left(\frac{U_{(T_s-T_{in})}}{T_s-T_{in}}\right)^2} \tag{13}$$

The uncertainty of heat flux and average heat transfer coefficient was estimated to be ± 6.7% and ± 7.8% at the heat flux of 50 W/cm^2 and the flow rate of 250 ml/min.

3. Results and discussions

As a pumping device, the flow rate and power consumption of the JAICIPM were experimentally tested at different driving voltages and frequencies. As shown in Fig. 6(a), the flow rate increases with the increase of the driving voltage because of larger vibrating amplitude of piezoelectric vibrator, but the power consumption grows rapidly too. The flow rate achieves 138.6 mL/min at 100 Vpp with a power consumption of 23 mW. The maximum flow rate achieves 306 mL/min at 300 Vpp with a power consumption of 232 mW. According to Eq. (9), the average jet velocity is proportional to the flow rate, ranging from 0.73 to 1.62 m/s in the experiments. As for the output pressure of the JAICIPM, it increases linearly with the driving voltage and achieves the maximum pressure of 32 kPa at 300 Vpp. As shown in Fig. 6(b), the flow rate increases first and then decreases with the increase of driving frequency. The maximum flow rate was obtained at 45 Hz. The power consumption at different frequencies shares the same trend with the flow rate below 70 Hz but continues to rise at a higher frequency. It can be concluded that changing driving voltage is more energy-efficient than changing the driving frequency when adjusting the flow rate of the JAICIPM.

The thermal performance of the JAICIPM was tested at different heat loads and driving voltages. The driving frequency is set to 45 Hz to get the best performance. The inlet temperature was maintained within 25∼30 °C, and surface temperature rise was controlled below 45 °C in the experiments. As shown in Fig. 7(a), the heat transfer coefficient increases with the increase of the driving voltage and heat load. When the driving voltage is 100 Vpp, the maximum heat load achieves 200 W, which means that 200 W heat load can be dissipated with a power consumption of 23 mW. And the HTC rises from 8843 W/(m^2·K) to 11,090 W/(m^2·K) with the increase of heat load. When the driving voltage is 200 Vpp, the maximum heat load achieves 301 W, and the HTC rises to 17,241 W/(m^2·K). The highest heat transfer coefficient of 20,572 W/(m^2·K) was achieved at 300 Vpp and 366 W. As mentioned above, a higher flow rate can be obtained with a higher driving voltage, which increases the jet velocity. Meanwhile, the temperature of the water near the cooling surface continues to rise with the increase of heat load, reducing the viscosity of the water. And the higher jet velocity and smaller viscosity increase the local Reynold number. Therefore, a thinner boundary layer can be obtained, resulting in a higher heat transfer coefficient. The calculated thermal resistance at different heat loads and driving voltages is shown in Fig. 7(b). When the driving voltage is 100 Vpp, the thermal resistance varies from 0.225 K/W to 0.283 K/W with the change of heat load. With the increase of driving voltage, the thermal resistance decreases obviously. When rising the driving voltage to 200 Vpp, the thermal resistance could drop to 0.145 K/W. The lowest thermal resistance of 0.122 K/W is obtained at 300 Vpp and 366 W.

To get the influence of the driving voltage clearer, the thermal performance of the JAICIPM at 200 W is shown in Fig. 7(c). As the driving voltage increases, the HTC increases and the surface temperature decreases. The curve of the HTC is similar to the flow

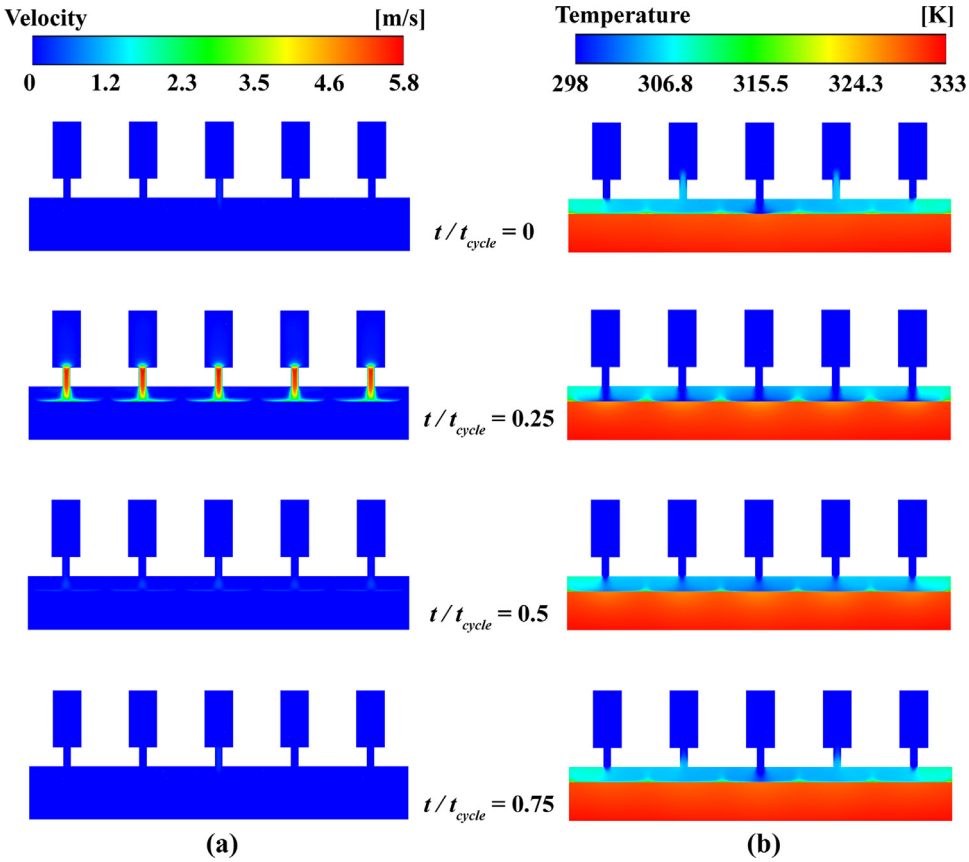

Fig. 11. Fields of the JAICIPM at different times: (a) velocity field, (b) temperature field.

Table 4
Performance of the liquid cooling systems driven by piezoelectric micropumps.

Author	Type	Pump size (mm)	Q_{max} (mL/min)	P_{max} (kPa)	Heat load (W)
Yueh [22]	Non-integrated	30 × 15 × 3.8	7	50	8
Lu [37]	Non-integrated	270 × 55 × 28	251.1	60.2	12.8
Ma [38]	Integrated	/	141	6.4	60
Tang [28]	Integrated	50 × 45 × 12	210	/	80
This work	Integrated	40 × 40 × 10	306	32	366

rate at different driving voltages, which increases rapidly first and then slows down. The surface temperature rise is 45 °C when the driving voltage is 100 Vpp. When the driving voltage increases to 300 Vpp, the wall temperature rise decreases to 27.2 °C.

Due to the unsteady jet impingement, the heat transfer coefficient and the surface temperature is changing through the cycles. Numerical simulations were performed to investigate the transient thermal performance. For the convenience of comparison, the heat load was set to 200 W and the flow rate was set to 150 ∼ 300 mL/min. The transient flow rate change was achieved with an UDF by changing the inlet velocity. The results from simulations and experiments were compared with the average heat transfer coefficient. As shown in Fig. 7(d), the simulations agree well with the experiments with a difference within 5%.

The Nusselt number *Nu* as a function of Reynolds number *Re* is shown in Fig. 8. The Nusselt number and Reynolds number were calculated based on the jet diameter. In this study, the Reynolds number ranged from 335 to 1054, and the Nusselt number ranged from 5.8 to 12.7. Non-linear fitting of these two parameters were performed, and the fitting result is

$$Nu = 0.075Re^{0.75} \tag{14}$$

As shown in Table 4, the performance of the JAICIPM is compared with the reported liquid cooling systems driven by piezoelectric micropumps. The non-integrated system means that piezoelectric micropump and heat sink are separated. While the integrated system means that piezoelectric micropump and heat sink are integrated. Results show the JAICIPM has a much better heat dissipation ability than other studies. At the same time, the JAICIPM remains small and consumes little electricity.

To investigate the transient heat transfer process of the JAICIPM, the case of 250 mL/min was analyzed in detail. The numerically calculated transient heat transfer coefficient and surface temperature rise are shown in Fig. 9. At $0 \sim 0.5\ t_{cycle}$, the coolant is ejected onto the cooling surface. When $t = 0$, the flow rate is zero and the surface temperature is high. With the increase of flow rate, the heat transfer coefficient increases to 27,969 W/(m^2·K) at $0.3\ t_{cycle}$. At this period, the surface temperature increases slightly and then decreases significantly. The jet impinging is finished at $0.5\ t_{cycle}$, and the HTC continues to decrease to 8547 W/(m^2·K) at $1\ t_{cycle}$. The surface temperature rise varies from 31.05 to 31.97 K in the cycle, and the time-averaged surface temperature rise is 31.52 K. Therefore, the average heat transfer coefficient is calculated as 15863 W/(m^2·K). The variation of surface temperature rise

is within 1 K, which indicates the stable cooling performance of the JAICIPM.

The temperature field of the cooling surface at different times is shown in Fig. 10. The surface temperature distribution keeps changing at different times. When $t = 0$, the surface temperature is high in all areas. When $t = 0.25\ t_{cycle}$, the temperature field shows a typical array jet cooling pattern, and the surface temperature in the jet area is much lower. Because of the arrangement of the nozzles, few coolants flow through the corners. And the flow rate distribution of jet nozzles is a little different due to the hydraulic resistance of the channels, which affects the temperature distribution too. Therefore, the highest temperature appears at the corner near the outlet. As time goes by, the jet velocity reduces and the temperature rises in the jet area. The temperature difference is within 6 K through the whole cycle. The cooling performance is uniform due to the jet array design.

To explain the process further, the velocity field and the temperature field were also studied. Fig. 11 shows the velocity field and the temperature field of the JAICIPM at different times. When $t = 0$, the jet velocity remains zero, and the temperature of the chip and the water nearby is high. When $t = 0.25\ t_{cycle}$, high-speed water is ejected onto the surface and then spreads, cooling down the surface and bringing in the low-temperature water. The average jet velocity achieves the maximum of 4.2 m/s and a thin thermal boundary is formed. Although the jet ends at $0.5\ t_{cycle}$, the temperature of the water near the surface remains relatively low. At $0.5 \sim 1\ t_{cycle}$, the heat of the chip is mainly dissipated by the heat conduction between the chip and the water nearby. It can be seen that the temperature of the water nearby continues to rise from $0.5\ t_{cycle}$.

4. Conclusions

In this work, we designed a compact jet array impingement cooling system driven by integrated piezoelectric micropump. The JAICIPM provides a high thermal performance and reduces the size of thermal management system by integrating jet impingement cooling with piezoelectric micropump. The liquid cooling system was designed, fabricated, and tested. A maximum convective heat transfer coefficient $h = 20{,}572\ W/m^2{\cdot}K$ is achieved at a heat flux of 91.5 W/cm^2. Furthermore, the JAICIPM is highly adjustable for different heat loads. A low temperature rise of 45 °C can be maintained under the heat load of 200 W when operated at 100 Vpp with an electric power consumption of 23 mW. The JAICIPM achieved a high thermal performance with a small size, and may become a promising option for cooling electronics in compact systems.

Declaration of Competing Interest

The authors declare no known competing financial interests or personal relationships that could have appeared to influence the work reported in this paper.

CRediT authorship contribution statement

Yiwen Fan: Conceptualization, Methodology, Data curation, Investigation, Software, Validation, Writing – original draft, Writing – review & editing. **Xinfeng Zhang:** Methodology, Investigation, Software. **Linyi Xiang:** Data curation, Formal analysis, Validation. **Yanhua Cheng:** Investigation, Writing – review & editing. **Xiaobing Luo:** Conceptualization, Funding acquisition, Project administration, Writing – review & editing.

Data Availability

No data was used for the research described in the article.

Acknowledgments

This work was supported by the National Natural Science Foundation of China (51625601).

Supplementary materials

Supplementary material associated with this article can be found, in the online version, at doi:10.1016/j.ijheatmasstransfer.2023.123905.

References

[1] S. Pu, J. Fu, Y. Liao, L. Ge, Y. Zhou, S. Zhang, S. Zhao, X. Liu, X. Hu, K. Liu, J. Chen, Promoting energy efficiency via a self-adaptive evaporative cooling hydrogel, Adv. Mater. 32 (2020) 1907307.
[2] B. Xie, H. Liu, R. Hu, C. Wang, J. Hao, K. Wang, X. Luo, Targeting cooling for quantum dots in white QDs-LEDs by hexagonal boron nitride platelets with electrostatic bonding, Adv. Funct. Mater. 28 (2018) 1801407.
[3] S. Yang, D. Xiang, A. Bryant, P. Mawby, L. Ran, P. Tavner, Condition monitoring for device reliability in power electronic converters: a review, IEEE Trans. Power Electron. 25 (2010) 2734–2752.
[4] M. Kim, H.-.P. Park, J.-.H. Jung, Hybrid input power balancing method of modular power converters for high efficiency, high reliability, and enhanced dynamic performance, IEEE Trans. Ind. Electron. 69 (2022) 5132–5141.
[5] F. Hou, H. Zhang, D. Huang, J. Fan, F. Liu, T. Lin, L. Cao, X. Fan, J.A. Ferreira, G. Zhang, Microchannel thermal management system with two-phase flow for power electronics over 500 W/cm^2 heat dissipation, IEEE Trans. Power Electron. 35 (2020) 10592–10600.
[6] X.D. Zhang, X.H. Yang, Y.X. Zhou, W. Rao, J.Y. Gao, Y.J. Ding, Q.Q. Shu, J. Liu, Experimental investigation of galinstan based minichannel cooling for high heat flux and large heat power thermal management, Energy Convers. Manag. 185 (2019) 248–258.
[7] M. Shi, X. Yu, Y. Tan, X. Wang, X. Zhang, J. Li, Thermal performance of insulated gate bipolar transistor module using microchannel cooling base plate, Appl. Therm. Eng. 201 (2022) 117718.
[8] Y. Wang, N.Y. Zhou, Z. Yang, Y.L. Jiang, Experimental investigation of aircraft spray cooling system with different heating surfaces and different additives, Appl. Therm. Eng. 103 (2016) 510–521.
[9] R. Xu, G. Wang, P. Jiang, Spray cooling on enhanced surfaces: a review of the progress and mechanisms, J. Electron. Packag. 144 (2022) 010802.
[10] G. Liang, I. Mudawar, Review of spray cooling - Part 1: single-phase and nucleate boiling regimes, and critical heat flux, Int. J. Heat Mass Transf. 115 (2017) 1174–1205.
[11] R.K. Wu, Y.W. Fan, T. Hong, H. Zou, R. Hu, X.B. Luo, An immersed jet array impingement cooling device with distributed returns for direct body liquid cooling of high power electronics, Appl. Therm. Eng. 162 (2019) 114259.
[12] T. Wei, H. Oprins, V. Cherman, J. Qian, I. De Wolf, E. Beyne, M. Baelmans, High-efficiency polymer-based direct multi-jet impingement cooling solution for high-power devices, IEEE Trans. Power Electron. 34 (2019) 6601–6612.
[13] L.L. Liu, X.C. Zhu, H. Liu, Z.H. Du, Effect of tangential jet impingement on blade leading edge impingement heat transfer, Appl. Therm. Eng. 130 (2018) 1380–1390.
[14] X. Wang, B. Li, D. Gerada, K. Huang, I. Stone, S. Worrall, Y. Yan, A critical review on thermal management technologies for motors in electric cars, Appl. Therm. Eng. 201 (2022) 117758.
[15] X.-.H. Yang, S.-.C. Tan, J. Liu, Thermal management of Li-ion battery with liquid metal, Energy Convers. Manag. 117 (2016) 577–585.
[16] A.H. Khalaj, S.K. Halgamuge, A review on efficient thermal management of air- and liquid-cooled data centers: from chip to the cooling system, Appl. Energy 205 (2017) 1165–1188.
[17] S. Zimmermann, I. Meijer, M.K. Tiwari, S. Paredes, B. Michel, D. Poulikakos, Aquasar: a hot water cooled data center with direct energy reuse, Energy 43 (2012) 237–245.
[18] L.J. Jiang, S.L. Jiang, W.L. Cheng, Y.L. Nian, R. Zhao, Experimental study on heat transfer performance of a novel compact spray cooling module, Appl. Therm. Eng. 154 (2019) 150–156.
[19] G. Tang, Y. Han, B.L. Lau, X. Zhang, D.M.W. Rhee, Development of a compact and efficient liquid cooling system with silicon microcooler for high-power microelectronic devices, IEEE Trans. Compon. Packag. Manuf. Technol. 6 (2016) 729–739.
[20] J. Ning, X. Wang, Y. Sun, C. Zheng, S. Zhang, X. Zhao, C. Liu, W. Yan, Experimental and numerical investigation of additively manufactured novel compact plate-fin heat exchanger, Int. J. Heat Mass Transf. 190 (2022) 122818.
[21] B. Duan, T. Guo, M. Luo, X. Luo, Ieee, a mechanical micropump for electronic cooling, in: Proceedings of the 14th InterSociety Conference on Thermal and Thermomechanical Phenomena in Electronic Systems (ITherm), Orlando, FL, 2014, pp. 1038–1042.
[22] W. Yueh, Z. Wan, H. Xiao, S. Yalamanchili, Y. Joshi, S. Mukhopadhyay, Active fluidic cooling on energy constrained system-on-chip systems, Ieee Trans. Compon. Packag. Manuf. Technol. 7 (2017) 1813–1822.
[23] K.W. Jung, C.R. Kharangate, H. Lee, J. Palko, F. Zhou, M. Asheghi, E.M. Dede, K.E. Goodson, Embedded cooling with 3D manifold for vehicle power elec-

tronics application: single-phase thermal-fluid performance, Int. J. Heat Mass Transf. 130 (2019) 1108–1119.
[24] B. Kwon, N.I. Maniscalco, A.M. Jacobi, W.P. King, High power density air-cooled microchannel heat exchanger, Int. J. Heat Mass Transf. 118 (2018) 1276–1283.
[25] R. Van Erp, R. Soleimanzadeh, L. Nela, G. Kampitsis, E. Matioli, Co-designing electronics with microfluidics for more sustainable cooling, Nature 585 (2020) 211–216.
[26] Y.H. Peng, D.H. Wang, X.Y. Li, Y. Zhang, Cooling chip on PCB by embedded active microchannel heat sink, Int. J. Heat Mass Transf. 196 (2022) 123251.
[27] L.Y. Zhang, Y.F. Zhang, J.Q. Chen, S.L. Bai, Fluid flow and heat transfer characteristics of liquid cooling microchannels in LTCC multilayered packaging substrate, Int. J. Heat Mass Transf. 84 (2015) 339–345.
[28] Y. Tang, M. Jia, X. Ding, Z. Li, Z. Wan, Q. Lin, T. Fu, Experimental investigation on thermal management performance of an integrated heat sink with a piezoelectric micropump, Appl. Therm. Eng. 161 (2019) 114053.
[29] H. Li, J. Liu, K. Li, Y. Liu, A review of recent studies on piezoelectric pumps and their applications, Mech. Syst. Signal Process 151 (2021) 107393.
[30] A. Nisar, N. Aftulpurkar, B. Mahaisavariya, A. Tuantranont, MEMS-based micropumps in drug delivery and biomedical applications, Sens. Actuators B Chem. 130 (2008) 917–942.
[31] H.K. Ma, B.R. Chen, J.J. Gao, C.Y. Lin, Development of an OAPCP-micropump liquid cooling system in a laptop, Int. Commun. Heat Mass Trans. 36 (2009) 225–232.
[32] D.J. Laser, J.G. Santiago, A review of micropumps, J Micromech. Microeng. 14 (2004) R35–R64.
[33] Y. Fan, W. Zhao, X. Zhang, X. Yu, X. Luo, Development of a piezoelectric pump with unfixed valve, J. Micromech. Microeng. 32 (2022) 055004.
[34] S.V. Ekkad, P. Singh, A modern review on jet impingement heat transfer methods, J. Heat Transf. Trans. Asme 143 (2021) 064001.
[35] H.C. Cui, J.H. Xie, R.Z. Zhao, M.Z. Wang, Z.C. Liu, W. Liu, Thermal-hydraulic performance analysis of a hybrid micro pin-fin, jet impingement heat sink with non-uniform heat flow, Appl. Therm. Eng. 208 (2022) 118201.
[36] H.C. Cui, X.T. Lai, J.F. Wu, M.Z. Wang, W. Liu, Z.C. Liu, Overall numerical simulation and experimental study of a hybrid oblique-rib and submerged jet impingement/microchannel heat sink, Int. J. Heat Mass Transf. 167 (2021) 120839.
[37] S. Lu, M. Yu, C. Qian, F. Deng, S. Chen, J. Kan, Z. Zhang, A quintuple-bimorph tenfold-chamber piezoelectric pump used in water-cooling system of electronic chip, IEEE Access 8 (2020) 186691–186698.
[38] H.K. Ma, B.R. Hou, C.Y. Lin, J.J. Gao, The improved performance of one-side actuating diaphragm micropump for a liquid cooling system, Int. Commun. Heat Mass Transf. 35 (2008) 957–966.